Research on the damage resilience model of a new steel-concrete inclined column transfer structure

Sen Tang[a,b] ID**, Zongyan Xie[c]** ID**, Bo Shen[a,b*]** ID**, Kejian Ma[a,b]** ID**, Tianhong Zheng[a,b]** ID

[a]Research Center of Space Structures, Guizhou University, China. Email: tsm18285649891@163.com, bshen@gzu.edu.cn, makejian2002@163.com, zth0730@163.com
[b]Key Laboratory of Structural Engineering of Guizhou Province, Guiyang 550025, China.
[c]China Railway Construction Real Estate Guizhou Co., Ltd, China. Email: 627004877@qq.com

* Corresponding author

https://doi.org/10.1590/1679-78258013

Abstract

For the new type of steel-concrete inclined column transfer structure (NSCICTS) with better lateral stiffness and ductility, the existing damage model and hysteresis model are difficult to accurately express the asymmetry of its test restoring force curve and the serious pinching phenomenon of the hysteresis curve, respectively. In this paper, an asymmetric damage model is firstly established according to the asymmetry of the curve, and the comparison with the existing symmetric damage model shows that the asymmetric damage model proposed can reflect the actual damage of the component or structure. Then, a simplified hysteresis loop model with a longer slip segment is established, and the damage formulas of the stiffness and residual deformation are established. Finally, the hysteresis rules are given, and the comparison with the test hysteresis curve shows that the proposed model can better simulate the structural mechanical properties. The model provides a theoretical basis for the overall nonlinear seismic analysis of the NSCICTS and other similar structures.

Keywords

New inclined column transfer structure; Damage model; Hysteresis curve; Pinching effect; Axial compression ratio

Graphical Abstract
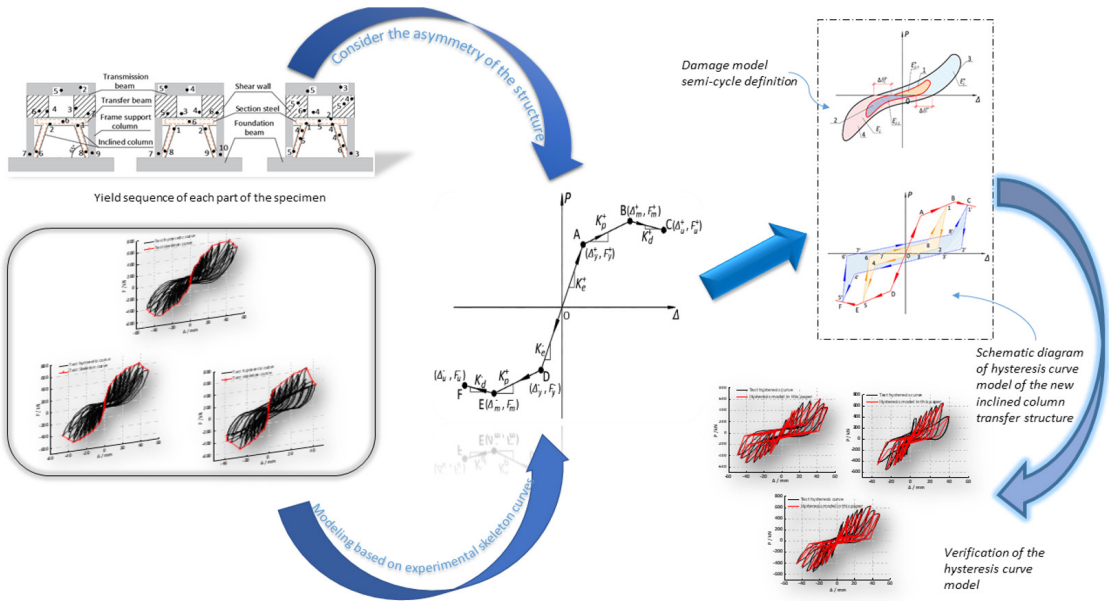
1 INTRODUCTION

In concrete high-rise buildings, a transfer layer is required between the upper shear wall and the lower frame column (Su and Cheng 2009, Pilz, S.E. et al. 2019). Currently, in engineering, the reinforced concrete inclined column transfer structure (RCICTS) is generally adopted. Lu, Z.A. (2018) makes a comparative analysis of RCICTS and the solid belly beam transfer structure from the aspects of period, displacement, stiffness ratio, and section size of the transfer beam, etc, the results show that the transfer structure of reinforced concrete inclined column can enhance the lateral stiffness of the transfer layer and the superstructure by direct transfer force, and effectively avoid the formation of weak layer. The elastic-plastic time-history analysis of RCICTS was carried out in (Zhao, S.L. et al. 2020), and the study showed that the seismic performance of the whole structure and each component could be improved by strengthening the construction of the inclined column joints. The inclined column joint was carried out in (Hua, H.Y. 2022), and it was found that the most unfavorable axial force did not necessarily appear when the plate thickness was zero, the fiber finite element software was used to verify the inclined column joint, and a practical design process for the inclined column joint was proposed. Some studies have shown that the application of traditional RCICTS in frame-supported short-leg shear wall structures has the following problems: 1) the damage to the net span section of the transfer beam between inclined columns is more serious; 2) The ductility and energy dissipation of RCICTS are lower than those of reinforced concrete beam transfer structures (Zhong, S.S. et al. 2007, QI, Y. et al. 2012). Based on the above problems, in order to improve the seismic performance of traditional RCICTS, strengthen the ductility of the transfer beam section between inclined columns, and make RCICTS more widely used in practical engineering, the research group proposes a new type of inclined column transfer structure with steel sections (NSCICTS), as shown in Figure 1. The NSCICTS is to arrange steel sections in the transfer beam and inclined column, and the NSCICTS has a steel-reinforced concrete transfer beam and a steel-reinforced concrete inclined column. The steel-reinforced concrete inclined columns can improve the lateral stiffness of the transfer layer, and the steel section of the transfer beam between inclined columns can be used as the main energy-dissipating beam segment. The test study of vertical constant load and horizontal reciprocating displacement loading was completed with the axial compression ratio changed and other geometric dimensions, reinforcement, and section steel unchanged (Zhang, J. et al. 2021, Li et al. 2015). According to the test results, the hysteresis curve and skeleton curve of a single specimen have obvious left-right asymmetry, and the pinching of the hysteresis curve is serious. To apply the NSCICTS to high-rise concrete building structures, it is particularly important to establish a restoring force model for seismic analysis of the NSCICTS according to the characteristics of its hysteresis curve and skeleton curve.

Damage variable which is defined by the ratio of the cumulative amount of a certain physical quantity to its limit allowable amount in the response process, can describe the damage degree of a component or structure. Structures under the action of earthquakes will produce different degrees of damage, with the accumulation of damage, and the mechanical properties such as strength and stiffness of the structure will continuously decrease, which will lead to structural damage. Since the nature of structural damage under seismic action is caused by the accumulation of irreversible damage, and the damage performance of the structure determines the seismic performance of the structure (Wei, B.C.et al. 2018), it is necessary to consider the damaging effect of the structure into the restoring force model.

At present, there are mainly the following damage variable models. Park and Ang (1985) assume that the load-displacement relationship of a structure under monotonic loading conforms to the ideal rigid-plastic model, and according to the ratio of ultimate deformation under seismic action to ultimate deformation under monotonic loading, and a linear combination of the ratio of the hysteretic energy under seismic action to the total energy under monotonic loading, a linear damage model is proposed, as shown in formula (1). Chen, L.Z. et al. (2010) proposed a modified form of the Park-Ang model, in which the total energy under monotonic loading is adopted as that of the ideal elastic-plastic model, as shown in formula (2). Zheng et al. (2012) proposed that the ultimate deformation under monotonic loading again after half-cycle loading minus the initial yield deformation replaces the ultimate deformation in the (Park and Ang, 1985) under monotonic loading; the total energy under monotonic loading again is taken as the total energy in the (Park and Ang, 1985) under the monotonic loading, and the model is similar to the ideal elastic-plastic model, as shown in formula (3). Qi, Z.Y. et al. (2016) further proposed that, without relying on the results of monotonic loading tests, the ultimate deformation under monotonic loading in the (Park and Ang, 1985) is changed to the ultimate deformation of the unidirectional skeleton curve obtained under low cycle reciprocating loading minus its initial cracking deformation, and the total energy under monotonic loading is changed to the total energy of the unidirectional skeleton curve, as shown in formula (4). It can be seen that the denominators of the deformation and energy terms in the above literature have only considered the indexes of monotonic or unidirectional load-displacement curves, and have not considered the difference between the indexes of load-displacement curves in the positive and negative directions. Then these damage models are symmetric damage variables and cannot consider the asymmetry of damage. Given this, it is necessary to establish a new damage model based on the stress characteristics of the NSCICTS.

At present, relevant scholars have carried out a large number of tests and theoretical research on the restoring force model of various reinforced concrete components or structures, and the common skeleton curve models are divided into curve type and folded line type. The curve type has a higher computational accuracy but the formula is complicated and not easy to use, which makes the folded line type more application. The Clough hysteresis model proposed by Clough and Johnston (1966) considers the stiffness degradation during reloading, and the unloading stiffness is equal to the yield (initial) stiffness, which is widely used for flexural components with shuttle-shaped hysteresis curves. Tohma and Hwang (1987) showed that the modified Takeda model to describe components or structures with shear deformation can better reflect the main characteristics of hysteresis curves with a pinching effect (as shown in Figure 5(a)), and the model is simple and easy to use, but it is not suitable for hysteresis curves with severe pinching. Based on the test results of the shear wall, the Ozcebe shear hysteresis model was established by Ozcebe and Saatcioglu (1989), which is a more commonly used hysteresis model considering the pinching effect, as shown in Figure 5(b), the unelastic unloading reaches the zero point of the load, with this zero point as the starting point for pinching. Then, the model pinches in reverse, and the load at the endpoint of pinching is the cracking load. Mazza F. (2019) proposed a nonlinear model based on plasticity and damage mechanism for seismic analysis of unelastic structures. By comparing the restoring force model with constant damage index and the restoring force model with variable damage index, the variable damage index was obtained, which could more accurately describe the cyclic degradation performance of structures. Carrero T. et al. (2020) conducted a cyclic loading test study on three types of CLT hybrid nodes, and established a restoring force model by considering six kinds of stiffness: elastic stiffness, elasto-plastic stiffness with hardening during loading, elasto-plastic stiffness with softening at advanced deformations of loading, unloading stiffness, reloading stiffness and continued unloading stiffness. Zuo Y. et al. (2021) considered the characteristics of stiffness degradation, strength degradation, slip phenomenon and pinch effect in the hysteretic curve of the test, and 7 feature points were defined to establish a multilinear restoring force model by analyzing the skeleton curve and hysteretic curve of the test. The assumptions of the pinching start and pinching endpoints in the above literature are different from the test results of the NSCICTS in this paper, and the pinching slip segment of the hysteresis loop of this test is longer than that of the model in the (Ozcebe and Saatcioglu 1989, Zhang and Yang 1999), i.e., the hysteresis loop of the NSCICTS has a more serious pinch effect, so the model in the above literature is no longer applicable. Given this, it is necessary to establish a new hysteresis curve model to address the establishment of a restoring force model in similar situations (Li, H.N. et al.2020, Wang, T. et al. 2021, Hu, S. et al. 2024).

This article establishes the skeleton curve model of the structure using a three-line model based on the asymmetric hysteresis curve and skeleton curve obtained from the test of three NSCICTS. Based on the skeleton curves, a new two-parameter damage model considering the asymmetry is proposed, which uses the skeleton curves as the load-displacement model. Then, a new hysteresis curve model is proposed according to the phenomenon that the test hysteresis curve has a long slip segment. By comparing with the test results, the damage-based hysteresis curve model is verified, which provides a theoretical basis for the elastic-plastic time-history analysis of NSCICTS and a computational model for other similar structures.

2 TEST RESULTS AND MODEL ESTABLISHMENT IDEAS OF THE NSCICTS

2.1 Test results

In the test, three 1/6 scale-down models were designed and fabricated, numbered MT1, MT2, and MT3 respectively, with corresponding axial compression ratios n of 0.2, 0.25, and 0.3 respectively, and the angles of the inclined columns were all 65°. Each specimen consists of six parts, including a transfer beam, frame support column, inclined column, shear wall, transmission beam and foundation beam (Zhang, J et al. 2021), as shown in Figure 1. Two 400kN mechanical jacks were applied to both sides of the transmission beams to simulate the vertical concentrated load of the self-weight of the superstructure, and one 1000kN servo actuator (MTS) was applied to the right side of the transmission beams to simulate the horizontal recurrent displacement loading of the seismic action. The whole process of test loading adopts displacement loading, with displacement increment Δ =1.12mm, and each cycle is loaded three times. The cyclic loading after yielding of MT1, MT2 and MT3 are 14Δ, 17Δ, 20Δ, 25Δ, 30Δ, 14Δ, 17Δ, 20Δ, 25Δ, 30Δ, 35Δ, 40Δ, 14Δ, 17Δ, 20Δ, 25Δ, 30Δ, 35Δ, 40Δ, respectively.

During the loading process of the three groups of specimens, plastic hinges were easily formed at the junction of the transfer beam and the inclined column, and at the foot of the frame pillar and the inclined column, in which the damage in the middle of the transfer beam and the transmission beam was more serious than that in other positions, and there were penetrating cracks on both sides in the inclined column and the foot of the frame pillar. The yield sequence of steel bars in each part of specimen MT1, MT2 and MT3, as shown in Figure 1 (a), (b), (c); specimen MT1,

MT2, and MT3 actual broken diagrams as shown in Figure 2 (a), (b), (c); hysteresis curves of the three specimens as shown in Figure 3 (a), (b), (c), all of which are "anti-S" type and have obvious pinching effect. From Figures 1, 2, and 3, it can be seen that the yielding sequence of steel bars, failure mode, skeleton curve, and hysteresis curve in the three specimens have obvious left-right asymmetry, which is due to the different damage of the left and right parts of the structure.
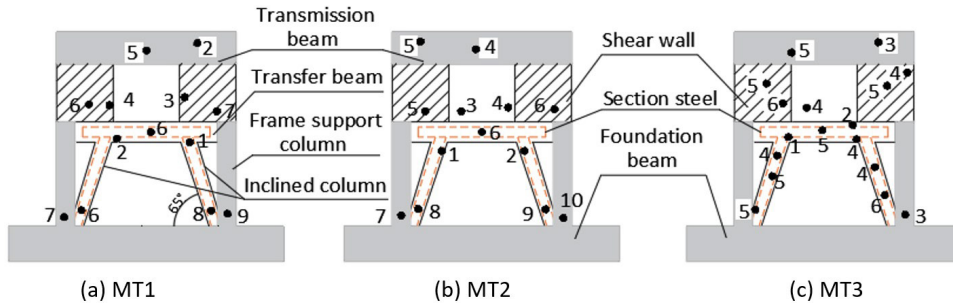

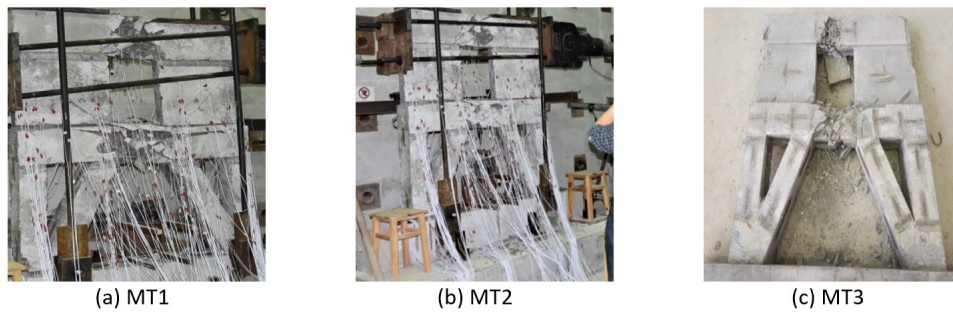**Figure 1** Yield sequence of each part of the specimen.

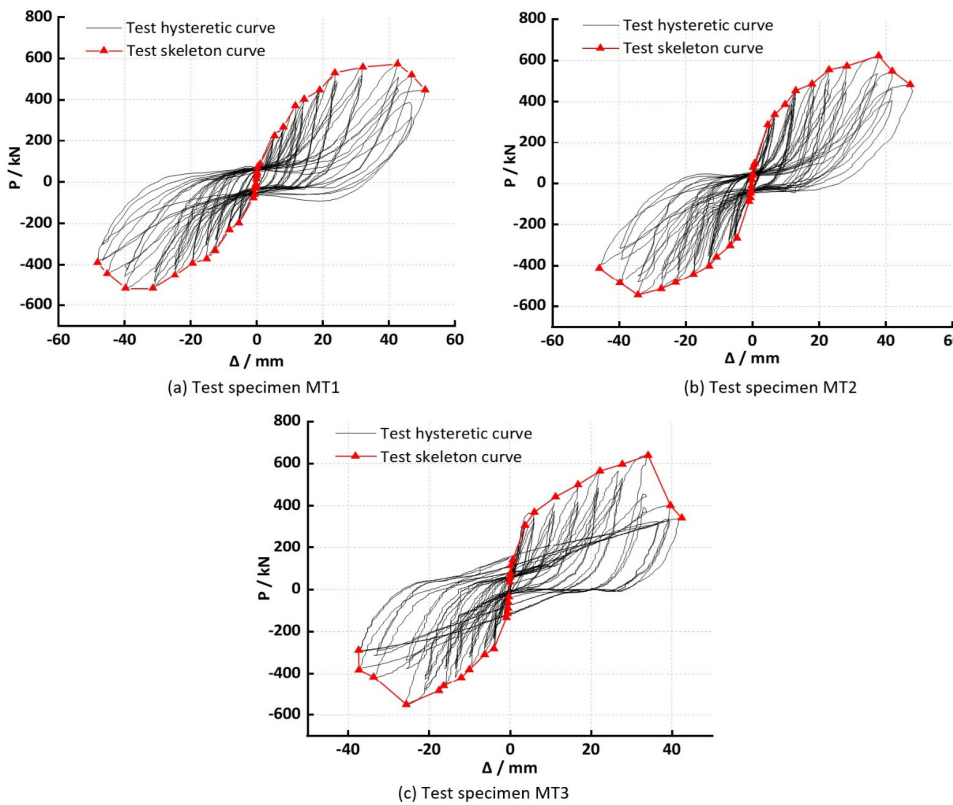**Figure 2** Actual diagram of specimen failure.

Figure 3 Hysteretic and skeleton curve of the test model

2.2 Establishment ideas for damage models

The damage models established in the Park and Ang (1985), Chen, L.Z. et al. (2010), Zheng, S.S. et al. (2012), Qi, Z.Y. et al. (2016) are as follows:

$$D_i = \frac{\delta_{im}}{\delta_u} + \beta \frac{\int dE_i}{P_y \delta_u} \tag{1}$$

$$D_i = (1 - \beta) \frac{\delta_{im}}{\delta_u} + \beta \frac{\int dE_i}{P_y(\delta_u - \delta_y)} \tag{2}$$

$$D_i = (1 - \beta) \sum_{j=1}^{N_1 \Sigma \int} \frac{(\frac{dE_i}{E_{iu}})^c}{(\frac{\delta y_{jmax}}{\delta_{iu} - \delta_y{}^c})} \tag{3}$$

$$D_i = \beta \frac{\delta_{im} - \delta_{cr}}{\delta_u - \delta_{cr}} + \gamma \frac{\int dE_i}{E_n} \tag{4}$$

Where: D_i is the damage index of the ith half-cycle; δ_{im} is the maximum deformation up to the ith half-cycle; δ_{jmax} in formula (3) is the deformation corresponding to the jth half-cycle (if it is the maximum deformation up to the jth half-cycle, the value is the maximum deformation for this purpose; otherwise, the first term on the right side of the equals sign of formula (3) is zero); dE_i is the hysteresis dissipation of the ith half-cycle; δ_y is the yield displacement under monotonic loading; δ_u is the ultimate deformation under monotonic loading; δ_{iu} and E_{iu} are the ultimate deformation and energy dissipation after loading the ith half-cycle again monotonically; P_y is the yield load under monotonic loading; δ_{cr}, δ_u, and E_n in formula (4) are the initial cracking deformation, ultimate deformation, and its energy dissipation of the unidirectional skeleton curve obtained by low- cycle repeated loading, respectively, and N_1 is the number of half-cycles that produce the maximum deformation δ_{jmax} for the first time, β and γ are the combination coefficients, and C is the test parameter.

The limit allowable amount of deformation index in formula (1) is the maximum deformation of the ideal rigid plasticity model, and the limit allowable amount of energy index is the maximum energy of the ideal rigid plasticity model, as shown in Figure 4 (a); it is essentially considered that the dynamic load-displacement of the component or structure obeys the model of ideal rigid-plasticity. The deformation index limit allowances of formulas (2) and (3) are the maximum deformation of ideal elastoplasticity and the maximum residual deformation of ideal elastoplasticity, and the limit allowances of energy indexes are the maximum energy of ideal elastoplasticity, as shown in Figure 4 (b); these two formulas essentially consider that the dynamic load-displacement of the component or structure obeys the ideal elastoplasticity model. The limit allowable amount of deformation index in formula (4) is the limit deformation of the unidirectional skeleton curve minus the initial cracking deformation, and the limit allowable amount of energy index is the energy of the unidirectional skeleton curve, as shown in Figure 4 (c); it is essentially considered that the dynamic load-displacement of the component or structure obeys the model of skeleton curve.

(a) The model of ideal rigid-plasticity   (b) The model of ideal elastoplasticity   (c) The unidirectional skeleton curve
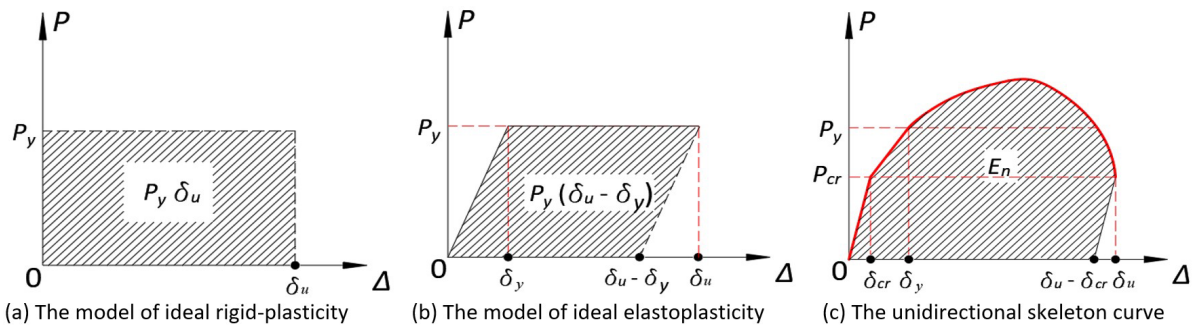
Figure 4 Model of damage variables

Taking the deformation index and energy index of the skeleton curve as the index limit allowable values ensures that the sources of the numerator and denominator of the damage variables are unified in the test results under cyclic loading, which can truly reflect the damage degree of the structure under cyclic loading. Formula (4) focuses on the cracking of the specimen and introduces the cracking deformation, however, for most of the structures, the yield deformation is an important factor to

consider the structural damage. The denominator terms of the above damage variable models all consider the indicators of monotonic or unidirectional load-displacement curves as the limit allowable values, which is essentially a symmetric damage model. For the structures in this paper, and most structures with symmetric geometry and symmetric reinforcement, the skeleton curves are asymmetric (Hung, C.C. et al. 2013), so it is necessary to improve the formula (4). The skeleton curve is divided into positive and negative segments, and the damage variables are divided into positive and negative damage. The deformation and energy index limit allowable values of the positive damage variable are the maximum residual deformation and energy of the skeleton curve in the positive direction, respectively. The deformation and energy term numerator of the positive damage variable are the residual deformation and hysteresis energy dissipation of each positive half hysteresis loop, respectively; the deformation and energy index limit allowable values of the negative damage variable are the maximum residual deformation and energy of the skeleton curve in the negative direction, and the deformation and energy term numerator of the negative damage variable are the residual deformation and hysteresis dissipation of each negative half hysteresis loop, respectively. The deformation and energy term numerator of the negative damage variable are the residual deformation and hysteresis energy dissipation of each negative half hysteresis loop, respectively.

2.3 Establishment ideas for the hysteresis loop model considering the pinching effect

The pinching effect of a hysteresis loop in concrete components or structure is caused by the sliding of two cracked surfaces, which were formed during the previous loading process. It is generally believed that the starting point of pinching is the zero point of unloading, such as point A or C in Figure 5, and the end point of the pinching is on the skeleton curve or at the point where the cracking load is reached, such as point B or D in Figure 5. However, as shown in Figure 5, the pinching starting point of the test hysteresis loop is A 'or C' point, and the pinching endpoint is B 'or D' point, which indicates that the modified Takeda hysteresis loop model (Tohma and Hwang 1987) and Ozcebe hysteresis loop model (Ozcebe and Saatcioglu 1989) are not suitable for the test hysteresis loops in this paper, and a new hysteresis loop model needs to be established.

In this paper, according to the characteristics of the test hysteresis loop, the endpoint of inelastic unloading is considered to be the starting point of pinching, and the starting point of reverse reloading is considered to be the end point of pinching, as shown in point A' (point C') and point B' (point D') in Figure 5. The straight line connecting the starting and ending points passes through the residual deformation point, and the slope of this straight line is the pinching stiffness. The area of the test hysteresis loop and the area of the hysteresis loop model in this paper are equal to determine the pinching stiffness so that the starting point and the endpoint of the pinching can be better matched with the test, which can actually reflect the sliding process of the NSCICTS.

(a) The hysteresis loop pinching model of modified Takeda   (b) The hysteresis loop pinching model of Ozcebe
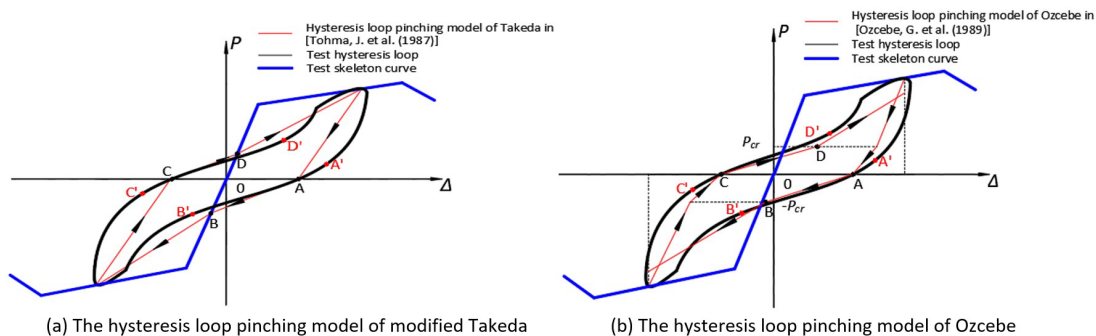
Figure 5 Existing hysteresis loop pinching model

3 ESTABLISHMENT OF SKELETON CURVE MODEL

Since the cracking points of the skeleton curves of specimens MT1, MT2 and MT3 in Figure 3 are not obvious, in this paper, the load applied at the end of the transmission beam when the strain of the transfer beam reinforcement reaches the yield strain for the first time (at 14Δ) is taken as the yield load, and the displacement at this time is taken as the yield displacement. Due to the difference between the positive and negative skeleton curves, a three-fold line skeleton curve model with elastic segments (OA, OD), strength-hardening segments (AB, DE), and strength-degradation segments (BC, EF) is adopted as shown in Figure 6. The skeleton curve model includes the following six key points, namely yield points A and D, peak load points B and E, and limit points C and F.
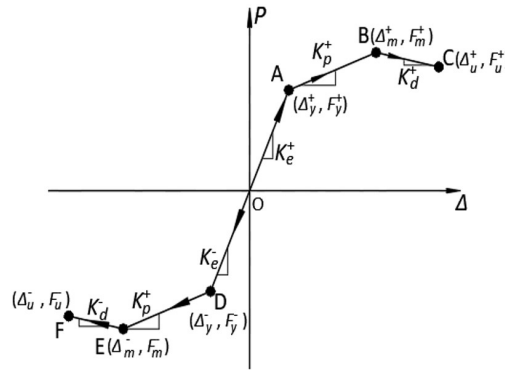
Figure 6 Trilinear model of skeleton curve

Regression analysis is carried out on the test skeleton curves to determine the coordinates of the six key points of the skeleton curve model and the fitting calculation formulas for elastic stiffness, hardening stiffness, and softening stiffness, which are shown in the Appendix (A-1.1~A-1.11). The calculated key point coordinates of the skeleton curve are shown in Table 1, and the error between the fitted calculated values of the six key point coordinates and the test values is less than 10%. The comparison between the calculated skeleton curves and the tested skeleton curves is shown in Figure 7, which shows that the trilinear skeleton curve model adopted in this paper can better describe the stress performance of the NSCICTS under seismic action.

Table 1 Calculated values of coordinates fitted to key points of skeleton curves of each specimen

Loading direction	Specimen	Δ_y^+ (mm)	F_y^+ (kN)	Δ_m^+ (mm)	F_m^+ (kN)	Δ_u^+ (mm)	F_u^+ (kN)
Forward loading	MT1	11.95	378.90	43.28	597.64	48.31	507.45
	MT2	11.68	396.88	37.94	620.24	43.10	527.85
	MT3	11.46	412.20	34.08	639.34	39.80	542.30
Loading direction	**Specimen**	Δ_y^- (mm)	F_y^- (kN)	Δ_m^- (mm)	F_m^- (kN)	Δ_u^- (mm)	F_u^- (kN)
Reverse loading	MT1	-12.81	-348.57	-40.74	-524.91	-46.22	-443.43
	MT2	-11.90	-369.58	-32.09	-541.89	-40.20	-466.98
	MT3	-9.51	-387.33	-26.41	-556.19	-32.70	-469.20

(a) Specimen MT1

(b) Specimen MT2
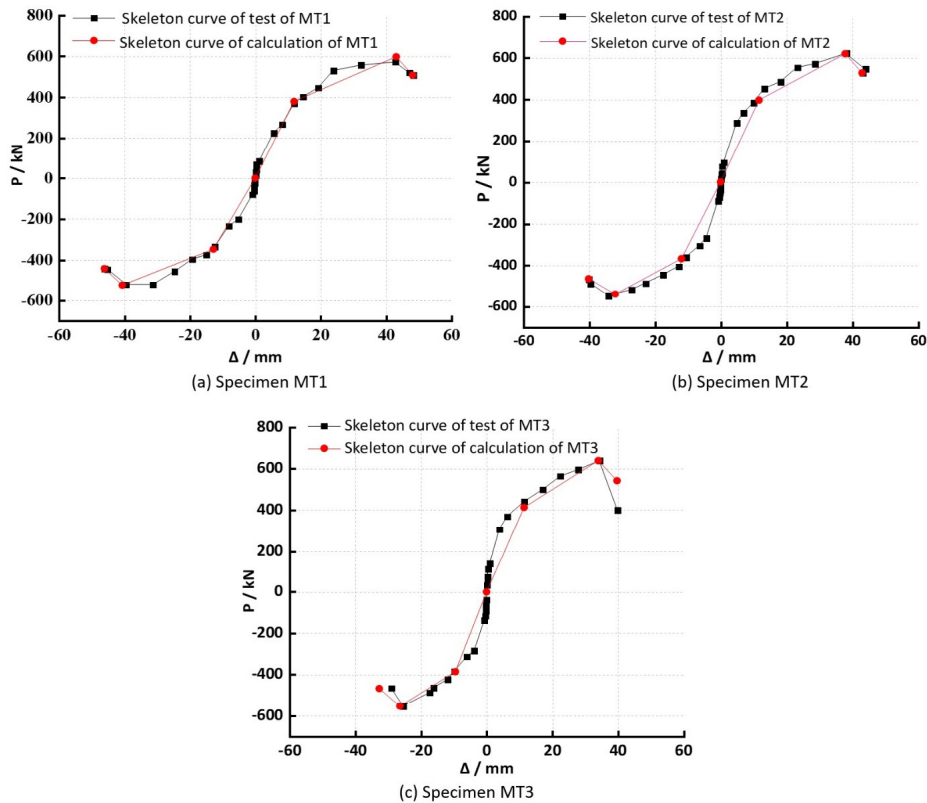

(c) Specimen MT3

Figure 7 Comparison of calculated and experimental skeleton curves

4 DAMAGE MODEL OF THE NSCICTS

4.1 Establishment of damage model

Based on the above analysis, this paper proposes a damage model considering the asymmetry of structural forces, which assumes that the damage $D = 0$ before reaching the yield load, and the damage begins to develop after reaching the yield load. The model expression is as follows:

$$\Delta D_i^{\pm} = (1 - \gamma)(\frac{\Delta \delta_i^{p\pm}}{\delta_p^{\pm}})^c + \gamma(\frac{E_i^{\pm}}{E_n^{\pm}})^c \tag{5}$$

$$D_j = \sum_{i=1}^{j} \Delta D_i^{\pm} \tag{6}$$

Where: $\Delta D_i^{\pm}$ is the damage increment of positive and negative half-cycle of level i^{th}; $\Delta \delta_i^{p\pm}$ is the residual deformation increment of positive and negative half-cycle of level i^{th} and level $(i-1)^{th}$, which is zero if the absolute value of residual deformation of level i^{th} is smaller than the absolute value of residual deformation of level $(i-1)^{th}$; $\delta_p^{\pm}$ is the residual deformation of unloading point of the skeleton curve in the positive and negative directions; $E_i^{\pm}$ is the hysteresis energy dissipation of positive and negative half-cycle of level i^{th}; $E_n^{\pm}$ is the energy dissipation of positive and negative direction of the skeleton curve; γ is the combination coefficient; and C is the test parameter.

The residual deformation increment and energy dissipation of positive and negative half cycles in the damage increment formula are defined as shown in Figure 8, where 1 is the positive half cycle of the $(i-1)^{th}$ cycle, and 2 is its negative half cycle; 3 is the positive half cycle of the ith cycle, and 4 is its negative half cycle. Figure 9 is the skeleton curve, the unloading starting point is determined as follows: get the slope of the straight line connecting the peak load point A(A') and the limit point B(B'), draw a straight line at the point B(B') according to this slope, and the intersection point of this straight line and the yield load B is the unloading starting point C(C'). The unloading stiffness is taken as elastic stiffness $K_y^{\pm}$. The denominator in the damage increment formula is taken according to the residual deformation and energy dissipation values in the skeleton curve in Figure 9.
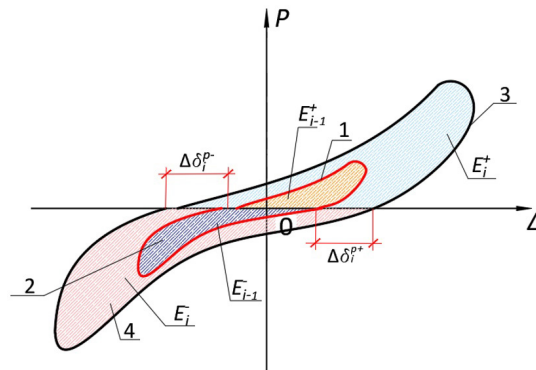

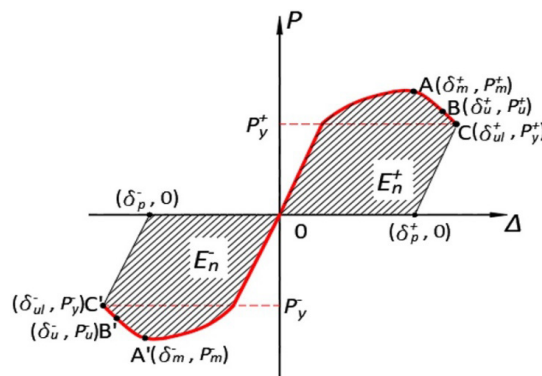**Figure 8** Damage model semi-cycle definition

Figure 9 The skeleton curve

4.2 Determination of the combination factor γ and test parameter C

Theoretically, when the damage index $D = 0$, the structure is in a non-destructive state; when the damage index $D = 1$, the structure is completely destroyed. The combination coefficient γ and test parameter C are introduced in formula (5) so that the damage index $D = 1$ when the structure is completely destroyed; the combination coefficient γ reflects the degree of contribution of the displacement term and energy term to the damage. These two parameters are determined as follows: firstly, the combination coefficient γ is determined, and the test parameter C is calculated from formula (6) when the damage index $D = 1$. After the analysis of the test data, when the combination coefficient $\gamma = 0.15$, the test parameters C of the three groups of specimens are relatively close, and the relationship between the test parameters C and the axial compression ratio n is given in Figure 10.
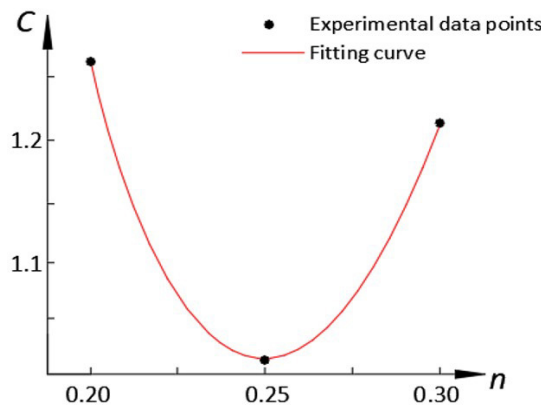

Figure 10 Relationship between test parameter C and axial pressure ratio n

As shown in Figure 10, it can be seen that the test parameter has a non-linear relationship with the axial compression ratio *n*. The expression is obtained by regression analysis as follows:

$$C = 83.526n^2 - 42.315n + 6.389, \quad R^2 = 1 \tag{7}$$

Where: $\boldsymbol{C}$-test parameter, *n*-axial pressure ratio

4.3 Validation of the damage model

The yield displacements of the three groups of specimens MT1, MT2, and MT3 are at 14Δ, and the maximum loading cycles of the three groups of specimens reach 30Δ, 40Δ, and 40Δ, respectively, when loading to failure. The damage began to develop after the structure reached the yield load, with 14Δ loading cycles as the level 1st, at this time, $D_1^{\pm} = 0$; after that, the damage began to develop, and the number of cycles calculated for MT1, MT2, and MT3 were level 5th, 7th, and 7th, respectively. In the case of combination coefficient $\gamma = 0.15$, the test parameters C of each specimen are calculated by formula (7), then the parameter $\delta_p^{\pm}$ and $E_n^{\pm}$ in the damage model are calculated, then the damage increment of each positive and negative half cycle is calculated by formula (5), and finally the damage variables are calculated by formula (6). The comparison of the results of the asymmetric damage model established in this paper and the symmetric damage model in the (Qi, Z.Y. et al. 2016) (note: for the comparison with the damage model in this paper, δ_{cr} in formula (4) is replaced by δ_y) is shown in Figure 11. It can be seen that the damage variables calculated in the (Qi, Z.Y. et al. 2016) are relatively small, which will underestimate the actual damage of the component or structure, especially in the early cycle of MT1 and MT2 damage, which shows that the asymmetric damage model proposed in this paper can reflect the actual damage of the component or structure.
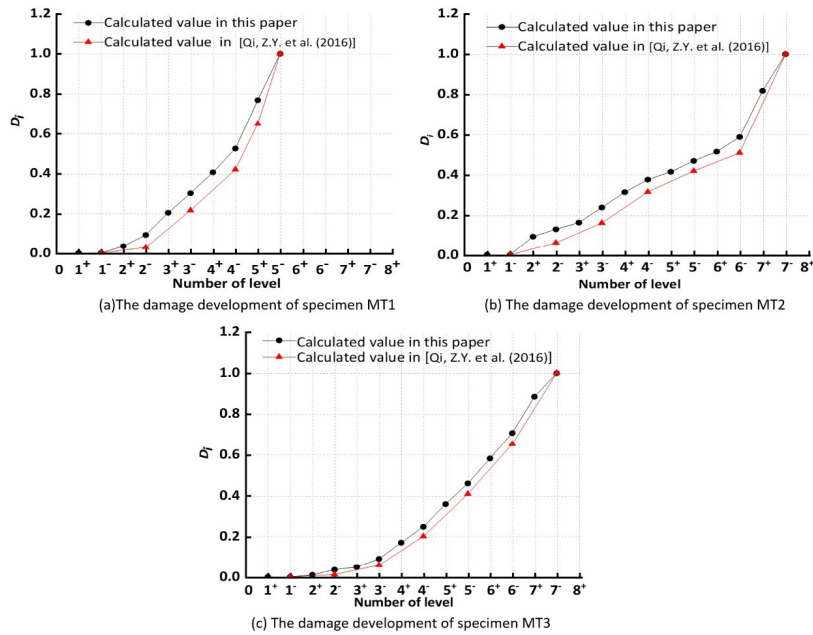
(a)The damage development of specimen MT1

(b) The damage development of specimen MT2

(c) The damage development of specimen MT3

Figure 11 Comparison of calculated values of damage

5 ESTABLISHMENT OF THE HYSTERESIS LOOP MODEL

5.1 Hysteresis loop simplification

The hysteresis loop of the NSCICTS after yielding has a long sliding section and serious pinching. According to the previous analysis, the simplified walking path of the ith cycle is shown in Figure 12. From point E → point A → point G → point B → point I → point C → point K → point D → point E on the skeleton curve, a cycle is completed. In Figure 12, point E is the peak load point of the positive cycle, the point I is the peak load point of the negative cycle, and its load value is equal to that of point E. Point G is the positive residual deformation point, and point K is the negative residual deformation point; the point L is the point very close to point E in the positive loading segment of the hysteresis curve, and the slope of the LE straight line is the positive loading stiffness K_{ir}^+; the point F is the point very close to point E in the positive unloading segment of the hysteresis curve, and the slope of the EF straight line is the positive unloading stiffness K_{iu}^+; Point H is the point very close to point I in the negative loading segment of the hysteresis curve, and the slope of the straight line HI is the negative loading stiffness K_{ir}^-; Point J is the point very close to point I in the negative unloading segment of the hysteresis curve, and the slope of the straight line IJ is the negative unloading stiffness K_{iu}^-. Points A and C are the starting point of the negative and positive pinching, respectively; and points B and D are the ending point of the negative and positive pinching, respectively; the slope of the straight line AB is the negative pinching stiffness K_{il}^-, and the slope of the straight line CD is the positive pinching stiffness K_{il}^+.
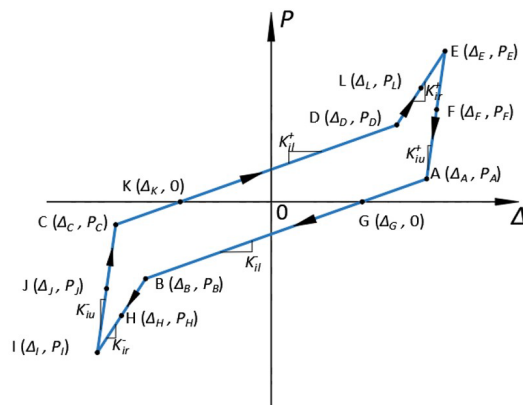

Figure 12 Establishment of the ith hysteresis loop model in this paper

The specific method is to find out the actual data of the above points L, E, F, G, H, I, J, and K in the test hysteresis loop, as well as the area of the positive and negative hysteresis loops. The simplified hysteresis loop should ensure that the simplified

positive area of the hysteresis loop is the same as the positive area of the test hysteresis loop, and the simplified negative area of the hysteresis loop is the same as the negative area of the test hysteresis loop, and then inversely calculated the positive pinching stiffness and negative pinching stiffness of the simplified hysteresis loop. Then two straight lines passing through point K and point G are obtained from the pinching stiffness, and the intersection of these two straight lines with the IJ line and EF line are determined, namely the positive pinching starting point C and the negative pinching starting point A. Determine the intersection of these two straight lines with the LE line and HI line, namely the positive pinching ending point D and the negative pinching ending point B. The specific calculation formula is shown in the Appendix (A-2.3~A-2.6).

5.2 Performance degradation analysis

Combined with the test data, it can be seen that with the loading and unloading, the loading, unloading, and pinching stiffness of the three groups of specimens gradually decreases, and the residual deformation gradually increases. This paper assumes that the structure starts to produce damage after yielding, and establishes a hysteresis loop model based on the damage of the loading, unloading, degradation of the pinching stiffness, and increase of the residual deformation.

Define the forward loading and unloading stiffness degradation law of the structure, and the reverse loading and unloading stiffness degradation law as follows:

$$K_{ir}^+ = (1 - \beta_{ir}^+)K_{i-1r}^+ \tag{8}$$

$$K_{iu}^+ = (1 - \beta_{iu}^+)K_{i-1u}^+ \tag{9}$$

$$K_{ir}^- = (1 - \beta_{ir}^-)K_{i-1r}^- \tag{10}$$

$$K_{iu}^- = (1 - \beta_{iu}^-)K_{i-1u}^- \tag{11}$$

Where: K_{ir}^+, K_{i-1r}^+ is the loading stiffness at the ith, $(i-1)^{th}$ cycle of forward loading, K_{iu}^+, K_{i-1u}^+ is the unloading stiffness at the ith, $(i-1)^{th}$ cycle of forward unloading; K_{ir}^-, K_{i-1r}^- is the loading stiffness at the ith, $(i-1)^{th}$ cycle of reverse loading, K_{iu}^-, K_{i-1u}^- is the unloading stiffness at the ith, $(i-1)^{th}$ cycle of reverse unloading; and β_{ir}^+, β_{iu}^+, β_{ir}^-, β_{iu}^- are the stiffness degradation coefficients of the ith cycle under forward loading, forward unloading, reverse loading and reverse unloading, respectively.

The stiffness degradation coefficient takes values between [0,1] and the closer its value is to 1, the more serious the degradation of the structural performance. Wang, B. (2010) defines the degradation coefficient, which is defined according to its idea, such as for β_{ir}^+, as follows:

$$\beta_{ir}^+ = (\frac{\Delta D_i^+}{1 - D_{i-1}^-})^\varphi$$

Where: ΔD_i^+ is the damage increment of the positive hysteresis loop in the ith cycle, $1 - D_{i-1}^-$ is the remaining damage value before the start of this forward hysteresis loop, and φ is the correlation coefficient. Fitting the calculation of β_{ir}^+ according to the above formula has $\varphi = 0.699$, and the coefficient of determination R^2 = 0.269, which indicates a poor fitting effect. In addition, the degradation coefficient β_{ir}^+ is defined using ΔD_i^+ in the above formula, but the ΔD_i^+ of the ith time is unknown, which is inconvenient to apply. Based on the above two problems, the derivation of the degradation coefficient formula in this paper is shown in the Appendix (A-3.1~A-3.8), and the results are as follows:

$$\beta_{ir}^+ = (\frac{\Delta D_{i-1}^-}{1-D_{i-1}^+} \cdot \frac{1}{\Delta D_{i-1}^+})^{C_r^+} \tag{12}$$

$$\beta_{iu}^+ = (\frac{\Delta D_{i-1}^-}{1-D_{i-1}^+} \cdot \frac{1}{\Delta D_{i-1}^+})^{C_u^+} \tag{13}$$

$$\beta_{ir}^- = (\frac{\Delta D_i^+}{1-D_{i-1}^-} \cdot \frac{1}{\Delta D_{i-1}^-})^{C_r^-} \tag{14}$$

$$\beta_{iu}^- = (\frac{\Delta D_i^+}{1-D_{i-1}^-} \cdot \frac{1}{\Delta D_{i-1}^-})^{C_u^-} \tag{15}$$

Where: ΔD_{i-1}^+ and ΔD_{i-1}^- are the damage increments of the positive and negative hysteresis loops in the $(i-1)^{th}$ cycle, respectively, ΔD_i^+ is the damage increment of the positive hysteresis loop in the ith cycle, D_{i-1}^+ is the total damage amount after the completion of the positive hysteresis loop in the $(i-1)^{th}$ cycle, and D_{i-1}^- is the total damage amount after the completion of the negative hysteresis loop in the $(i-1)^{th}$ cycle, and C_r^+, C_u^+, C_r^- and C_u^- are the fitted correlation coefficients.

From formula (12), it can be seen that the denominator term ΔD_{i-1}^+ reduces the fluctuation of the numerator term ΔD_{i-1}^-, which increases the coefficient of determination R^2 of formula fitting, and the fitting effect is better. In addition, the calculation of the degradation coefficient for this cycle relies on the damage variable values of previous cycles, which facilitates the application of the formula. The fitting calculation results of the correlation coefficient are shown in the Appendix (A-3.9~A-3.12).

After the yield of the structure, the residual deformation increases continuously, and the pinching stiffness degenerates continuously, and the definition is as follows:

$$\delta_i^{p+} = (1 + \beta_i^{p+})\delta_{i-1}^{p+} \tag{16}$$

$$\delta_i^{p-} = (1 + \beta_i^{p-})\delta_{i-1}^{p-} \tag{17}$$

$$K_{il}^+ = (1 - \beta_{il}^+)K_{i-1l}^+ \tag{18}$$

$$K_{il}^- = (1 - \beta_{il}^-)K_{i-1l}^- \tag{19}$$

Where: δ_{i-1}^{p+}, δ_{i-1}^{p+} are the positive and negative residual deformation of the $(i-1)^{th}$ cycle, respectively; δ_i^{p+}, δ_i^{p-} are the positive and negative residual deformation of the ith cycle, respectively; K_{i-1l}^+, K_{i-1l}^- are the positive and negative pinching stiffness of the $(i-1)^{th}$ cycle, respectively; K_{il}^+, K_{il}^- are the positive and negative pinching stiffness of the ith cycle, respectively; β_i^{p+}, β_i^{p-} are the coefficient of increase in the ith positive and negative residual deformation, respectively β_{il}^+, β_{il}^- are the degradation coefficient of the ith positive and negative pinching stiffness, respectively.

$$\beta_i^{p+} = \left(\frac{\Delta D_{i-1}^- + \Delta D_{i-1}^+}{D_{i-1}^+}\right)C^+ \tag{20}$$

$$\beta_i^{p-} = \left(\frac{\Delta D_i^+ + \Delta D_{i-1}^-}{D_{i-1}^-}\right)C^- \tag{21}$$

$$\beta_{il}^+ = \left(\frac{\Delta D_{i-1}^- + \Delta D_{i-1}^+}{1 - D_{i-1}^-}\right)C_l^+ \tag{22}$$

$$\beta_{il}^- = \left(\frac{\Delta D_i^+ + \Delta D_{i-1}^-}{1 - D_i^+}\right)C_l^- \tag{23}$$

Where: D_i^+ is the total damage amount after the completion of the positive hysteresis loop of the ith cycle, and the rest of the damage is the same as above; $C_{\square}^+$, $C_{\square}^-$, C_l^+ and C_l^- are the fitted correlation coefficients. The fitted calculations of the correlation coefficients are shown in the Appendix (A-3.13~A-3.16).

According to the correlation coefficients in the Appendix (A-3.13~A-3.16), the calculation results of formulas (12) to (15) and (20) to (23) are shown in Table 2. As can be seen from Table 2, the coefficients have no change law with the increase of the number of cycles, which is caused by the different damage values of each cycle.

Table 2: Coefficients calculated by fitting formulas for three groups of specimens

Specimen	Load loop	β_{ir}^+	β_{iu}^+	β_{ir}^-	β_{iu}^-	β_i^{p+}	β_i^{p-}	β_{il}^+	β_{il}^-
MT1	14Δ	0.040	0.040	0.146	0.070	0.230	0.217	0.161	0.152
	17Δ	0.048	0.048	0.169	0.136	0.279	0.186	0.154	0.131
	20Δ	0.046	0.046	0.050	0.118	0.293	0.172	0.161	0.181
	25Δ	0.052	0.052	0.332	0.179	0.143	0.162	0.161	0.152
	30Δ	0.052	0.052	0.236	0.183	0.148	0.171	0.156	0.126
MT2	14Δ	0.051	0.051	0.143	0.165	0.242	0.180	0.096	0.078
	17Δ	0.054	0.054	0.148	0.202	0.175	0.163	0.104	0.143
	20Δ	0.029	0.029	0.136	0.076	0.035	0.121	0.160	0.185
	25Δ	0.051	0.051	0.200	0.113	0.626	0.165	0.175	0.157
	30Δ	0.058	0.058	0.045	0.123	0.321	0.091	0.147	0.058
	35Δ	0.068	0.068	0.146	0.139	0.143	0.049	0.161	0.124
	40Δ	0.078	0.078	0.127	0.152	0.175	0.065	0.159	0.089
MT3	14Δ	0.068	0.068	0.133	0.138	0.146	0.046	0.115	0.147
	17Δ	0.097	0.097	0.175	0.180	0.162	0.081	0.136	0.135
	20Δ	0.029	0.029	0.109	0.094	0.182	0.259	0.147	0.164
	25Δ	0.081	0.081	0.106	0.115	1.258	0.329	0.160	0.188
	30Δ	0.093	0.093	0.201	0.119	1.214	0.244	0.179	1.022
	35Δ	0.160	0.160	0.073	0.133	0.588	0.068	0.146	0.135
	40Δ	0.187	0.187	0.216	0.137	0.294	0.064	0.210	0.315

6 HYSTERESIS CURVE MODEL AND ITS VERIFICATION

6.1 The proposal of hysteretic rule

According to the simplified model of the hysteresis loop established in this paper and its degradation calculation formula for each performance index based on damage, the hysteresis curve model of the NSCICTS is established, as shown in Figure 13. The hysteresis rules of the hysteresis curve model is:

(1) When the specimen is loaded and unloaded before reaching the yield point, the forward and reverse loading and unloading are loaded and unloaded according to the elastic stiffness, that is, walking along the OA (OD) segment in the figure.

(2) After the specimen is loaded to the yield point A, it walks along the skeleton curve until it reaches any point 1, and then walks along 1 (maximum load point in the positive direction of the cycle) → 2 (pinching starting point in the negative direction) → 3 (residual deformation point in the positive direction) → 4 (pinching ending point in the negative direction) → 5 (maximum load point in the negative direction of the cycle, which is equal to the load of point 1) → 6 (pinching starting point in the positive direction) → 7 (residual deformation point in the negative direction) → 8 (pinching ending point in the positive direction) → 1 to complete a cycle. According to the previous formula to calculate the loading stiffness, unloading stiffness, pinch stiffness, and residual deformation point, and to complete a cycle. Then continue to walk along the skeleton curve, continue the cycle, and calculate the loading stiffness, unloading stiffness, pinching stiffness, and residual deformation point.

(3) After the specimen is loaded to the peak load point B, it points to the ultimate displacement point C along the skeleton curve and unloads according to the degradation stiffness. After walking to any point 1', similar to (2), complete a cycle along 1' → 2'→ 3' → 4'→ 5' → 6'→ 7' → 8'→ 1'. Then continue to walk along the skeleton curve and continue the cycle until all cycles are completed. The loading stiffness, unloading stiffness, pinching stiffness, and residual deformation points are calculated in the cycle.
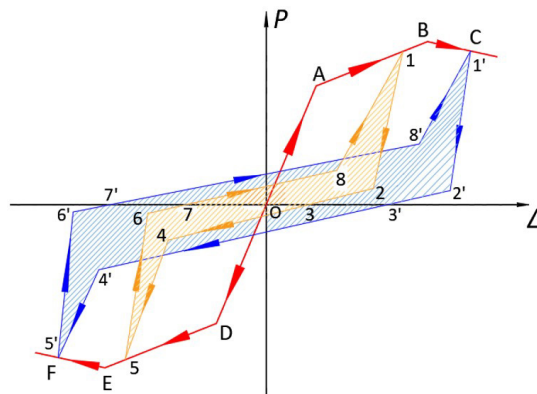

Figure 13 Schematic diagram of hysteresis curve model of the NSCICTS

6.2 Comparison of the hysteresis curve model and traditional model

Since the establishment of Ozcebe model needs to consider the cracking load, and the cracking load is often difficult to be determined in the test, inaccurate cracking load will also affect the accuracy of hysteresis model. Therefore, a hysteresis loop in MT1 was selected for comparison with the modified Takeda hysteresis model in this paper. As shown in Figure 14, it can be seen that the loading stiffness and unloading stiffness defined in this paper are in good agreement with the test hysteresis loop. In addition, the pinching stiffness determined in this paper by the equal area of the experimental hysteresis loop and the hysteresis loop model also accurately reflects the slip phenomenon of the hysteresis curve of NSCICTS, at the same time, the residual deformation defined based on damage is also partly in agreement with the test. However, the modified Takeda model does not consider the degradation of unloading stiffness, and the unloading stiffness of the model is consistent with the loading stiffness, so it can be seen that it is not applicable to the hysteretic curve with serious pinching in this paper.
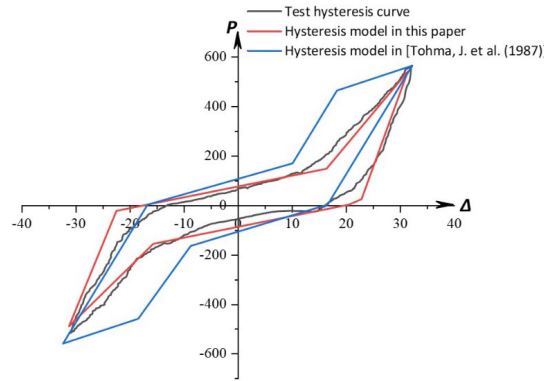
Figure 14 Comparison between hysteresis model in this paper and hysteresis model in modified Takeda

6.3 Comparison of the hysteresis curve model and experiment

According to the proposed hysteresis curve model, the calculated hysteresis curve of the NSCICTS can be obtained, which is compared with the experimental hysteresis curve, and the results are shown in Figure 15. The calculated curve is in good agreement with the test curve, indicating that the restoring force model proposed in this paper can effectively simulate the mechanical properties of the NSCICTS. The model provides a theoretical basis for the overall nonlinear analysis of the NSCICTS, and also provides a restoring force model for other similar structures.
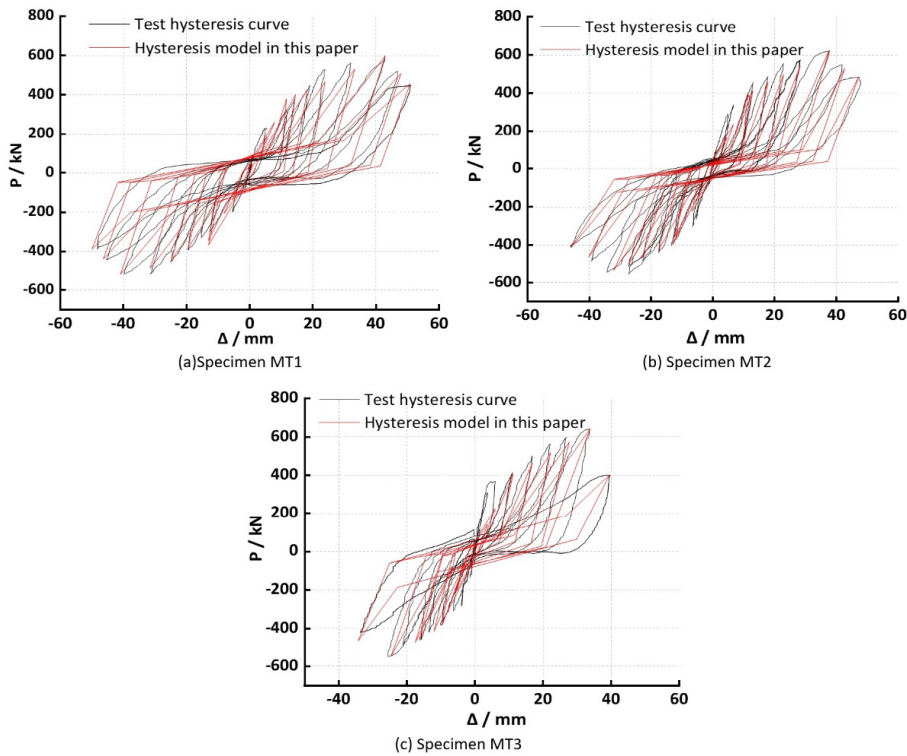

Figure 15 Comparison between calculated hysteresis curve and experimental hysteresis curve

7 CONCLUSION

This paper researchs the restoring force model based on the test results of the NSCICTS with low-cycle reciprocating loading, and the main conclusions are as follows:

(1) According to the characteristics of asymmetric stress performance of the NSCICTS, the damage model considering the asymmetric structural stress is established by taking the skeleton curve (load-displacement curve) as a model.

(2) Comparison of the asymmetric damage model in this paper with the existing symmetric damage model, the symmetric damage model underestimates the damage to the components or structures, and the asymmetric damage model can reflect the actual damage of the components or structure.

(3) According to the NSCICTS hysteresis loop has a long slip segment and serious pinching, this paper establishes the simplified model of the hysteresis loop and its degradation formula considering the loading, unloading, and pinching stiffness of damage, as well as the calculation formula of residual deformation increase.

(4) The hysteresis rule of the hysteresis curve is established in this paper, and the calculated hysteresis curves are in good agreement with the test hysteresis curves, which provides a theoretical basis for the elastic-plastic time-history analysis of the NSCICTS.

Author's Contribuitions: Conceptualization, Bo Shen; Methodology, Zongyan Xie; Investigation, Sen Tang; Writing-original draft, Sen Tang and Zongyan Xie; Writing-review & editing, Sen Tang; Funding acquisition, Bo Shen; Resources, Bo Shen and Kejian Ma; Supervision, Bo Shen and TianHong Zheng.

Editor: Rogério José Marczak

References

Su, R.K.L., Cheng, M.H. (2009). Earthquake-induced shear concentration in shear walls above transfer structures, Structural Design of Tall & Special Buildings, 18(6): 657-671.

Pilz, S.E., Ribeiro, R., Pilz, D., Pavan, R.C.,& Costella, M.F. (2019). Global stability analysis in reinforced concrete buildings with transfer beams, Structures & Buildings, 2019, 172(9): 685-699.

Lu, Z.A. (2018). Comparative analysis of mechanical properties in the core tube of frame with transfer layer between the solid-wed beam transfer and new type of inclined column transfer with shaped steel. In: Materials Science and Engineering Conference Series, 423: 012027.

Zhao, S.L., Zhu, Z.J., & Miao, J.R. (2020). Structural design and analysis of inclined column conversion at the bottom of a super high-rise building [J]. Journal of building structures, 50 (14) : 40-45 (in Chinese)

Hua, H.Y. (2022). Research on Design key points of Inclined column conversion of super tall structure [J]. Journal of building structures, 52(S2): 103-110. (in Chinese)

Zhong, S.S., Yang, C.L., & Lu, T. (2007). Seismic test analysis of inclined column and beam transfer story structures, Journal of Chongqing University (Natural Science Edition), (04): 56-60 (in Chinese)

QI, Y., Zhu, C.M., & Zhong, S.S. (2012). Experimental study on seismic performance of inclined column-shaped transfer floor structure of frame-supported short-leg shear wall based with various ratio leg-thickness, Journal of Vibration and Shock, 31(12): 155-159. (in Chinese)

Zhang, J., Fan, Y., Zhou, S., Shen, B., Ma, K., Wu, H., & Liu, B. (2021). Seismic behaviour of a steel-reinforced concrete inclined column transfer structure under different axial force ratios, Arabian Journal of Geosciences, 14(11):1046.

Li, M., Shen, B., Xie, C.J., Zhou, S.M., Zhao, Q.Y., & Long, H.F. (2015). Mechanical performance analysis of frame supported shear wall structures with new inclined column conversion, Journal of Guizhou University (Natural Science Edition), 32 (02): 94-98(in Chinese)

Wei, B.C., Zhang, J.S., Zhang, Y.H., & Zhou, J.L. (2018). Damage model of reinforced concrete members under cyclic loading, E3S Web of Conferences, 38: 03057.

Park, Y.J., Ang, A.H.S. (1985). Mechanistic seismic damage model for reinforced concrete, Journal of Structural Engineering,111(4): 722-739.

Chen, L.Z., Jiang, H.j., & Lv, X.l. (2010). Revised Park Ang damage model for reinforced concrete structures, Journal of Tongji University (Natural Science Edition), (8): 1103-1107 (in Chinese)

Zheng, S.S., Hou P.J., & Zhang, H.R. (2012). Experimental study on seismic damage of srhshpc frame structures, Engineering Mechanics, 29 (07): 84-92 (in Chinese)

Qi, Z.Y., Jiang, N., & Wang, L. (2016). Research on seismic damage model of new gypsum concrete composite wall panels. Vibration and Shock, 35 (19): 181-188 (in Chinese)

Clough, R.W., Johnston, S.B. (1966). Effect of stiffness degradation on earthquake ductility requirements, Proc. 2th Jappan Earth. Engng. Symp, Tokyo Japan

Tohma, J., Hwang, H. (1987). Hysteretic model for reinforced concrete containment, Transactions of the 9th International SMIRT Conference, Lousanne 17(1): 25-256.

Ozcebe, G., Saatcioglu, M. (1989). Hysteretic shear model for reinforced concrete members, Journal of Structural Engineering, 115(1), 132–148.

Mazza, F. (2019). A plastic-damage hysteretic model to reproduce strength stiffness degradation. Bulletin of Earthquake Engineering, 17(6), 3517-3544.

Carrero, T., Montaño, J., Santa-María, H., & Guindos, P. (2020). Static and dynamic performance of direct hybrid connections of cross-laminated timber with steel, concrete and laminated strand lumber composites. Latin American Journal of Solids and Structures, 17, e279.

Zuo, Y., Xu, Z., Chen, Z., & Dai, S. (2021). Restoring-force model for HFC-filled CFS shear walls subjected to in-plane cyclic loading. Journal of Building Engineering, 44, 103347.

Zhang, L.X., Yang, H. (1999). Shear hysteresis model of shear walls, World Earthquake Engineering, 15 (2): 9-16(in Chinese)

Li, H.N., Li, R.H., Li, C., & Wang, D.B. (2020). Development of hysteretic model with dynamic effect and deterioration for seismic-performance analysis of reinforced concrete structures. Journal of Structural Engineering, 146(10): 04020215.

Wang, T., Jiang, R., Yuan, S., Yuan, K., Li, L., & Zhou, G. (2021). A restoring force model for prefabricated concrete shear walls with built-in steel sections. Applied Sciences, 11(24): 12131.

Hu, S., Koetaka, Y., Chen, Z.P., Zhu, S., & Alam, M.S. (2024). Hybrid self-centering braces with NiTi-SMA U-shaped and frequency-dependent viscoelastic dampers for structural and nonstructural damage control. Engineering Structures, 308: 117920.

Hung, C.C., Su, Y.F., & Yu, K.H. (2013). Modeling the shear hysteretic response for high performance fiber reinforced cementitious composites, Construction and Building Materials, 41: 37-48.

Wang, B., M.Eng, Thesis (in Chinese) (2010). Research on seismic damage of high-strength and high-performance steel reinforced concrete components and their frame structures, Xi'an University of Architecture and Technology, Xian.

APPENDIX 1 – Data fitting and formula derivation.

Symbol	Meaning
Superscript "+", "–"	Represent the positive and negative directions of the skeleton curve and hysteresis loop respectively
$F_y^{\pm}$, $\Delta_y^{\pm}$	The yield load, and yield displacement of the skeleton curve, respectively
$F_m^{\pm}$, $\Delta_m^{\pm}$	Load and displacement at the peak load of the skeleton curve, respectively
$F_u^{\pm}$, $\Delta_u^{\pm}$	Load and displacement at the ultimate displacement of the skeleton curve, respectively
$K_e^{\pm}$, $K_p^{\pm}$, $K_d^{\pm}$	The elastic stiffness, hardening stiffness, and degradation stiffness of the skeleton curve, respectively

1 The fitting calculation formula for the coordinates and stiffness of key points in a three-line skeleton curve model

1.2 Fitting formula for yield loads and their displacements and elastic stiffness

Based on the test results the calculation formula was determined by software regression analysis as follows:

$$\Delta_y^+ = e^{2.315} \cdot n^{-0.103}, R^2 = 0.851 \tag{A-1.1}$$

$$\Delta_y^- = -e^{1.371} \cdot n^{-0.732}, R^2 = 0.991 \tag{A-1.2}$$

$$F_y^+ = e^{6.271} \cdot n^{0.208}, R^2 = 0.988 \tag{A-1.3}$$

$$F_y^- = -e^{6.270} \cdot n^{0.259}, R^2 = 0.973 \tag{A-1.4}$$

$$K_e^{\pm} = \frac{F_y^{\pm}}{\Delta_y^{\pm}} \tag{A-1.5}$$

Where: R^2 is the coefficient of determination of the statistic measuring the goodness of fit; n is the axial pressure ratio.

1.2 Fitting formula for peak loads and their displacements and hardening stiffness

The calculation formula is as follows:

$$\Delta_m^+ = e^{2.819} \cdot n^{-0.589}, R^2 = 0.998 \tag{A-1.6}$$

$$\Delta_m^- = -e^{1.986} \cdot n^{-1.069}, R^2 = 0.939 \tag{A-1.7}$$

$$F_m^+ = e^{6.661} \cdot n^{0.116}, R^2 = 0.997 \tag{A-1.8}$$

$$F_m^- = -e^{6.492} \cdot n^{0.413}, R^2 = 0.856 \tag{A-1.9}$$

$$K_p^{\pm} = \frac{F_m^{\pm} - F_y^{\pm}}{\Delta_m^{\pm} - \Delta_y^{\pm}} \tag{A-1.10}$$

1.3 Fitting formula for ultimate loads and their displacements and softening stiffness

The ultimate load $F_u^{\pm}$ is 0.85 times the peak load $F_m^{\pm}$, which is calculated as shown in formula (1.11), and the ultimate displacement $\Delta_u^{\pm}$ is calculated as shown in formula (1.12). The reduction coefficient is introduced to calculate the softening stiffness, and its calculation formula is shown in formulas (1.13) ~ (1.15).

$$F_u^{\pm} = 0.85 F_m^{\pm} \tag{A-1.11}$$

$$\Delta_u^{\pm} = \frac{0.15 F_m^{\pm}}{\alpha^{\pm} K_e^{\pm}} + \Delta_m^{\pm} \tag{A-1.12}$$

$$\alpha^+ = -18.297n^2 + 8.197n - 0.355, R^2 = 1 \tag{A-1.13}$$

$$\alpha^- = -12.095n^2 + 4.507n + 0.023, R^2 = 1 \tag{A-1.14}$$

$$K_d^{\pm} = \alpha^{\pm} K_e^{\pm} \tag{A-1.15}$$

2 Hysteresis loop pinching stiffness and pinching point coordinate solution

Let the positive loading stiffness of original hysteresis loop be $K_{ir}^+ = \dfrac{P_E - P_L}{\Delta_E - \Delta_L}$, the positive unloading stiffness be

$K_{iu}^+ = \dfrac{P_E - P_F}{\Delta_E - \Delta_F}$, the negative loading stiffness be $K_{ir}^- = \dfrac{P_I - P_H}{\Delta_I - \Delta_H}$, the negative unloading stiffness be $K_{iu}^- = \dfrac{P_I - P_J}{\Delta_I - \Delta_J}$. Let the

positive pinch stiffness be K_{il}^+ and the negative pinch stiffness be K_{il}^-.

According to Figure 12, the areas of the positive half cycle and negative half cycle are:

$$E_C^+ = 0.5(\Delta_D - \Delta_K)P_D + (\Delta_E - \Delta_D)P_D + 0.5(\Delta_E - \Delta_D)(\mathbf{P}_E - P_D) - 0.5(\Delta_A - \Delta_G)P_A - (\Delta_E - \Delta_A)P_A -$$
$$- 0.5(\Delta_E - \Delta_A)(P_E - P_A) \tag{A-2.1}$$

$$E_C^- = 0.5(\Delta_G - \Delta_B)(-P_B) + (\Delta_B - \Delta_I)(-P_B) + 0.5(\Delta_B - \Delta_I)(P_B - P_I) - 0.5(\Delta_K - \Delta_C)(-P_C) -$$
$$- (\Delta_C - \Delta_I)(-P_C) - 0.5(\Delta_C - \Delta_I)(P_C - P_I) \tag{A-2.2}$$

The positive and negative half cycle areas of the test hysteresis loop are E_T^+ and E_T^-, respectively. Let $E_C^+ = E_T^+$ and

$E_C^- = E_T^-$, and the pinching stiffness K_{il}^+ and K_{il}^- can be obtained. From the pinch stiffness, the coordinates of pinch

starting point and ending point can be obtained as follows:

$$\Delta_A = \frac{K_{il}^- \Delta_G - K_{iu}^+ \Delta_E + P_E}{K_{il}^- - K_{iu}^+} \quad , \quad P_A = \frac{K_{il}^-}{K_{il}^- - K_{iu}^+}(K_{iu}^+ \Delta_G - K_{iu}^+ \Delta_E + P_E) \tag{A-2.3}$$

$$\Delta_B = \frac{K_{il}^- \Delta_G - K_{ir}^- \Delta_I + P_I}{K_{il}^- - K_{ir}^-} \quad , \quad P_B = \frac{K_{il}^-}{K_{il}^- - K_{ir}^-}(K_{ir}^- \Delta_G - K_{ir}^- \Delta_I + P_I) \tag{A-2.4}$$

$$\Delta_C = \frac{K_{il}^+ \Delta_K - K_{iu}^- \Delta_I + P_I}{K_{il}^+ - K_{iu}^-} \quad , \quad P_C = \frac{K_{il}^+}{K_{il}^+ - K_{iu}^-}(K_{iu}^- \Delta_K - K_{iu}^- \Delta_I + P_I) \tag{A-2.5}$$

$$\Delta_D = \frac{K_{il}^+ \Delta_K - K_{ir}^+ \Delta_E + P_E}{K_{il}^+ - K_{ir}^+} \quad , \quad P_D = \frac{K_{il}^+}{K_{il}^+ - K_{ir}^+}(K_{ir}^+ \Delta_K - K_{ir}^+ \Delta_E + P_E) \tag{A-2.6}$$

3 Derivation of the expression of the cyclic degradation coefficient and calculation of its correlation coefficient
3.1 Derivation of expressions for cyclic degradation coefficient

Let: $K_{ir}^+ = (1 - D_i^+)K_e^+$, $K_{i-1r}^+ = (1 - D_{i-1}^+)K_e^+$,

that is: $\Delta K_{ir}^+ = \Delta D_i^+$, $\Delta K_{i-1r}^+ = \Delta D_{i-1}^+$, $\dfrac{K_{ir}^+}{K_{i-1r}^+} = \dfrac{1 - D_i^+}{1 - D_{i-1}^+} = \dfrac{1 - (D_{i-1}^+ + \Delta D_{i-1}^+ + \Delta D_i^+)}{1 - D_{i-1}^+}$, i.e. $\dfrac{K_{ir}^+}{K_{i-1r}^+} = 1 - (\dfrac{\Delta D_{i-1}^+ + \Delta D_i^+}{1 - D_{i-1}^+}) = 1 - \beta_{ir}^+$.

Let: $\dfrac{\Delta K_{ir}^+}{\Delta K_{i-1r}^+} = \dfrac{\Delta D_i^+}{\Delta D_{i-1}^+} = \alpha$, α is a constant

$$\beta_{ir}^+ = \frac{\Delta D_{i-1}^+ + \Delta D_i^+}{1 - D_{i-1}^+} = \frac{\Delta D_{i-1}^-}{1 - D_{i-1}^+}(1 + \frac{\Delta D_i^+}{\Delta D_{i-1}^-})(\frac{\Delta D_{i-1}^+}{\Delta D_{i-1}^+}) = \frac{\Delta D_{i-1}^-}{1 - D_{i-1}^+}\frac{1}{\Delta D_{i-1}^+}(\Delta D_{i-1}^+ + \frac{\Delta D_i^+ \Delta D_{i-1}^+}{\Delta D_{i-1}^-}) =$$

$$= \frac{\Delta D_{i-1}^-}{1 - D_{i-1}^+}\frac{1}{\Delta D_{i-1}^+}(\Delta D_{i-1}^+ + \frac{\alpha \cdot \Delta D_{i-1}^+ \Delta D_{i-1}^+}{\Delta D_{i-1}^-})$$

that is:

Let: $\Delta D_{i-1}^- = \beta \cdot \Delta D_{i-1}^+$, then simplify the above equation as follows:

$$\beta_{ir}^+ = \frac{\Delta D_{i-1}^-}{1 - D_{i-1}^+}\frac{1}{\Delta D_{i-1}^+}(\Delta D_{i-1}^+ + \frac{\alpha}{\beta}\Delta D_{i-1}^+)$$

Let: $(\Delta D_{i-1}^+ + \dfrac{\alpha}{\beta}\Delta D_{i-1}^+) = \varepsilon$, introduce correlation coefficients to construct the above equation as follows:

$\beta_{ir}^+ = (\varepsilon \cdot \dfrac{\Delta D_{i-1}^-}{1 - D_{i-1}^+} \cdot \dfrac{1}{\Delta D_{i-1}^+})^{C_r^+}$, at this point, let $\varepsilon = 1$ again to obtain the following formula:

$$\beta_{ir}^+ = (\frac{\Delta D_{i-1}^-}{1 - D_{i-1}^+} \cdot \frac{1}{\Delta D_{i-1}^+})^{C_r^+} \tag{A-3.1}$$

The formulas for the remaining coefficients β_{iu}^+, β_{ir}^- and β_{iu}^- are also similar to the above formula, namely:

$$\beta_{iu}^+ = (\frac{\Delta D_{i-1}^-}{1 - D_{i-1}^+} \cdot \frac{1}{\Delta D_{i-1}^+})^{C_u^+}$$

(A-3.2)

$$\beta_{ir}^- = (\frac{\Delta D_i^+}{1 - D_{i-1}^-} \cdot \frac{1}{\Delta D_{i-1}^-})^{C_r^-}$$

(A-3.3)

$$\beta_{iu}^- = (\frac{\Delta D_i^+}{1 - D_{i-1}^-} \cdot \frac{1}{\Delta D_{i-1}^-})^{C_u^-}$$

(A-3.4)

Let: $\delta_i^{p+} = D_i^+ \delta_1^{p+}$, $\delta_{i-1}^{p+} = D_{i-1}^+ \delta_1^{p+}$, that is:

$$\frac{\delta_i^{p+}}{\delta_{i-1}^{p+}} = \frac{D_i^+}{D_{i-1}^+} = \frac{D_{i-1}^+ + \Delta D_{i-1}^- + \Delta D_i^+}{D_{i-1}^+} = 1 + \frac{\Delta D_{i-1}^- + \Delta D_i^+}{D_{i-1}^+}$$

Let: $\Delta D_i^+ \approx \Delta D_{i-1}^+$, that is:

$$\frac{\delta_i^{p+}}{\delta_{i-1}^{p+}} = 1 + \beta_i^{p+} \approx 1 + \frac{\Delta D_{i-1}^- + \Delta D_{i-1}^+}{D_{i-1}^+}$$, introducing correlation coefficients to construct the above equation as follows:

$$\beta_i^{p+} = (\frac{\Delta D_{i-1}^- + \Delta D_{i-1}^+}{D_{i-1}^+})^{C^+}$$

(A-3.5)

And the formula for coefficient a is also similar to the above equation, namely:

$$\beta_i^{p-} = (\frac{\Delta D_i^+ + \Delta D_{i-1}^-}{D_{i-1}^-})^{C^-}$$

(A-3.6)

Similar to the above derivation, the degradation coefficient of pinching stiffness can be obtained as follows:

$$\beta_{il}^+ = (\frac{\Delta D_{i-1}^- + \Delta D_{i-1}^+}{1 - D_{i-1}^-})^{C_i^+}$$

(A-3.7)

$$\beta_{il}^- = (\frac{\Delta D_i^+ + \Delta D_{i-1}^-}{1 - D_i^+})^{C_i^-}$$

(A-3.8)

3.2 Fitting calculation results of correlation coefficients

The fitting calculation results of the correlation coefficient and its determination coefficient are as follows:

$$C_r^+ = 7.972 - \frac{0.190}{n^2} - \frac{2.670(\frac{\Delta D_{i-1}^-}{1 - D_{i-1}^+} \cdot \frac{1}{\Delta D_{i-1}^+})}{Ln(\frac{\Delta D_{i-1}^-}{1 - D_{i-1}^+} \cdot \frac{1}{\Delta D_{i-1}^+})} , R^2 = 0.997$$

(A-3.9)

$$C_u^+ = \frac{-3.403 + 11.708n + 3.065(\frac{\Delta D_{i-1}^-}{1 - D_{i-1}^+} \cdot \frac{1}{\Delta D_{i-1}^+})}{1 - 1.157n - 0.253(\frac{\Delta D_{i-1}^-}{1 - D_{i-1}^+} \cdot \frac{1}{\Delta D_{i-1}^+}) - 0.512(\frac{\Delta D_{i-1}^-}{1 - D_{i-1}^+} \cdot \frac{1}{\Delta D_{i-1}^+})^2} , R^2 = 0.998$$

(A-3.10)

$$C_r^- = -0.113 + 28.773n^2 - \frac{3.110}{Ln(\frac{\Delta D_i^+}{1 - D_{i-1}^-} \cdot \frac{1}{\Delta D_{i-1}^-})} , R^2 = 0.921$$

(A-3.11)

$$C_u^- = -0.106 + \frac{0.022}{n^2} - \frac{2.281}{Ln(\frac{\Delta D_i^+}{1 - D_{i-1}^-} \cdot \frac{1}{\Delta D_{i-1}^-})} , R^2 = 0.854$$

(A-3.12)

$$C^+ = -0.802 + 0.045n + 15.480(\frac{\Delta D_{i-1}^- + \Delta D_{i-1}^+}{D_{i-1}^+}) - 30.636(\frac{\Delta D_{i-1}^- + \Delta D_{i-1}^+}{D_{i-1}^+})^2 +$$

$$+ 14.899(\frac{\Delta D_{i-1}^- + \Delta D_{i-1}^+}{D_{i-1}^+})^3 - 2.106(\frac{\Delta D_{i-1}^- + \Delta D_{i-1}^+}{D_{i-1}^+})^4 , \quad R^2 = 0.978$$

(A-3.13)

$$C^- = -0.355 + 73.986n^3 - \frac{1.497}{Ln(\frac{\Delta D_i^+ + \Delta D_{i-1}^-}{D_{i-1}^-})} \ , \ R^2 = 0.924 \tag{A-3.14}$$

$$C_i^+ = 0.541 + 2.696n^{-0.741} - (\frac{\Delta D_{i-1}^+ + \Delta D_{i-1}^-}{1 - D_{i-1}^-})^{1.547} , \ R^2 = 0.928 \tag{A-3.15}$$

$$C_i^- = 0.486 + 3.021n^{-0.653} - (\frac{\Delta D_i^+ + \Delta D_{i-1}^-}{1 - D_i^+})^{1.747} , \quad R^2 = 0.954 \tag{A-3.16}$$